Cellular/Molecular

Vestibular Hair Bundles Control pH with $(Na^+, K^+)/H^+$ Exchangers NHE6 and NHE9

Jennifer K. Hill,[1] Christopher L. Brett,[2] Anthony Chyou,[2] Laura M. Kallay,[2] Masao Sakaguchi,[3] Rajini Rao,[2] and Peter G. Gillespie[1]

[1]Oregon Hearing Research Center and Vollum Institute, Oregon Health & Science University, Portland, Oregon 97239, [2]Department of Physiology, Johns Hopkins University, Baltimore, Maryland 21205, and [3]Graduate School of Life Science, University of Hyogo, Ako, Hyogo 678-1297, Japan

In hair cells of the inner ear, robust Ca^{2+}/H^+ exchange mediated by plasma-membrane Ca^{2+}-ATPase would rapidly acidify mechanically sensitive hair bundles without efficient removal of H^+. We found that, whereas the basolateral membrane of vestibular hair cells from the frog saccule extrudes H^+ via an Na^+-dependent mechanism, bundles rapidly remove H^+ in the absence of Na^+ and HCO_3^-, even when the soma is acidified. K^+ was fully effective and sufficient for H^+ removal; in contrast, Rb^+ failed to support pH recovery. Na^+/H^+-exchanger isoform 1 (NHE1) was present on hair-cell soma membranes and was likely responsible for Na^+-dependent H^+ extrusion. NHE6 and NHE9 are organellar isoforms that can appear transiently on plasma membranes and have been proposed to mediate K^+/H^+ exchange. We identified NHE6 in a subset of hair bundles; NHE9 was present in all bundles. Heterologous expression of these isoforms in yeast strains lacking endogenous exchangers conferred pH-dependent tolerance to high levels of KCl and NaCl. NHE9 preferred cations in the order K^+, $Na^+ \gg Rb^+$, consistent with the relative efficacies of these ions in promoting pH recovery in hair bundles. Electroneutral K^+/H^+ exchange, which we propose is performed by NHE9 in hair bundles, exploits the high-K^+ endolymph, responds only to pH imbalance across the bundle membrane, is unaffected by the +80 mV endocochlear potential, and uses mechanisms already present in the ear for K^+ recycling. This mechanism allows the hair cell to remove H^+ generated by Ca^{2+} pumping without ATP hydrolysis in the cell.

Key words: **hair cells; H^+; pH; NHE; ion transport; mechanotransduction**

Introduction

The plasma-membrane Ca^{2+}-ATPase (PMCA) isoform 2, essential for auditory and vestibular function (Kozel et al., 1998; Street et al., 1998), obligatorily countertransports H^+ in exchange for Ca^{2+} (Hao et al., 1994; Salvador et al., 1998). PMCA2 is present at ~2000 molecules/μm^{-2} in hair bundles of sensory hair cells (Yamoah et al., 1998), with the PMCA2v/a isoform located in frog vestibular hair bundles and the closely related PMCA2w/a in mammalian auditory and vestibular bundles (Dumont et al., 2001; Hill et al., 2006). When maximally activated, PMCA may transport Ca^{2+} at >1 mM/s (Yamoah et al., 1998); H^+ will similarly rise in hair bundles at 1 mM/s unless it is removed.

How do hair bundles handle H^+ influx? Although bundles presumably have endogenous H^+ buffers to blunt pH changes on a short timescale, sustained maintenance of neutral pH requires H^+ removal from the bundle. In somas of hair cells (Ikeda et al., 1992) and in many other cell types (Brett et al., 2005a), Na^+/H^+ exchangers (NHEs) transport H^+ across the plasma membrane, but Na^+-dependent exchangers cannot operate in hair bundles because of the lack of extracellular Na^+ in the endolymph. Although H^+ transport could be achieved by diffusion to the soma, this mechanism would generate transepithelial H^+ flow, requiring H^+ pumping to maintain pH in the endolymph, the K^+-rich extracellular solution bathing the bundles. When HCO_3^- is present, the Na^+-HCO_3^- cotransporter (Romero and Boron, 1999) or the HCO_3^-/Cl^- exchanger (Romero et al., 2004) might remove acid equivalents. Alternatively, some cells use proton pumps such as the V-type H^+-ATPase (Blair et al., 1989) and gastric or nongastric H^+/K^+-ATPases (Silver and Soleimani, 1999) to extrude H^+; these pumps are typically used to generate large transmembrane H^+ gradients, however, rather than to maintain equal pH on both sides of the membrane.

We demonstrate here that hair bundles regulate pH independently of the cell body, using a mechanism that operates in the presence of K^+. We identified two strong candidates for the bundle H^+ extrusion mechanism, both members of a subgroup of the NHE family, which are thought to use K^+ to maintain pH homeostasis in intracellular organelles. NHE6 and NHE9 were both detected in hair bundles, with NHE9 present on all bundles and NHE6 expressed on a subset of bundles. Both NHE6 and NHE9 were shown to mediate K^+/H^+ exchange by functional complementation in yeast. Because hair bundles are normally exposed to high-K^+ endolymph, these experiments suggest that

Received July 14, 2006; revised Aug. 14, 2006; accepted Aug. 16, 2006.

This work was supported by National Institutes of Health Grants R01 DC002368 (P.G.G.), R01 DC004571 (P.G.G.), P30 DC005893 (P.G.G.), R01 DK54214 (R.R.), and F31 DC05517 (J.K.H.).

Correspondence should be addressed to Peter G. Gillespie, L335A Auditory Neuroscience, Oregon Health & Science University, 3181 SW Sam Jackson Park Road, Portland, OR 97239. E-mail: gillespg@ohsu.edu.

J. K. Hill's present address: Department of Biology and Center for Comparative and Evolutionary Biology of Hearing, University of Maryland, College Park, MD 20742.

DOI:10.1523/JNEUROSCI.2990-06.2006

 0270-6474/06/269944-12$15.00/0

Table 1. Ionic composition of saline solutions (in mM)

Solutions	Na^+, TPA^+, or Rb^+	K^+	Ca^{2+}	Mg^{2+}	Cl^-	NH_4^+	$NMDG^+$	Glucose	HEPES
Standard saline	110	2	4	2	124	0	0	3	10
Low-Ca^{2+} saline	110	2	0.1	2	116	0	0	3	10
NH_4^+/NaCl	85	2	4	2	124	25	0	3	10
NH_4Cl/NMDG-Cl	0	2	4	2	124	25	85	3	10
NMDG-Cl/KCl/M^{2+}	0	2	4	2	124	0	110	3	10
NMDG-Cl/KCl	0	2	0	0	124	0	122	3	10
NMDG-Cl only	0	0	0	0	124	0	124	3	10
KCl only	0	124	0	0	124	0	0	3	10
TPA-Cl/KCl	122	2	0	0	124	0	0	3	10
TPA-Cl only	124	0	0	0	124	0	0	3	10
RbCl only	124	0	0	0	124	0	0	3	10

"M^{2+}" refers to divalent cations (Ca^{2+} and Mg^{2+}). All solutions were adjusted to pH 7.25 and were saturated with O_2.

bundles perform electroneutral K^+/H^+ exchange, allowing the exchange mechanism to maintain a constant pH in and outside stereocilia.

Materials and Methods

pH measurement. Experiments were performed at room temperature on bullfrog (*Rana catesbeiana*) saccular hair cells isolated as described previously (Hirono et al., 2004), using a low-Ca^{2+} saline solution (Table 1). Most hair cells of the frog saccule belong to one of two morphological types (Chabbert, 1997); although we mostly examined central cylindrical cells, we measured similar pH dynamics in central flask-shaped cells as well. Hair cells were loaded with the AM form of the pH-sensitive ratiometric dye 5-(and-6)-carboxylic acid seminapthorhodamine-5F (SNARF-5F) (Invitrogen, Carlsbad, CA). We used the related dye SNARF-1 in a few experiments with similar results. Saline solutions containing dye and Pluronic F-127 (10 μl of a 20% solution for each 20 nmol of dye; from Invitrogen) were prepared immediately before use. To load hair cells, saccules were incubated for 5 min with 3.3 μM dye SNARF-5F in low-Ca^{2+} saline solution supplemented with DNase I (50 μg/ml) and were then allowed to recover for 5 min in fresh 3.3 μM dye. After dissociation of hair cells, the low-Ca^{2+} dye solution was exchanged for standard saline solution containing 6.7 μM SNARF-5F. After 20 min, the dye solution was replaced with standard saline solution. Experiments with seminapthorfluorescein-calcein (SNAFL-calcein) used identical loading procedures.

Hair cells were viewed with a Plan Apo 60× (numerical aperture, 1.40) oil lens on a Nikon (Tokyo, Japan) TE 300 inverted microscope with a Bio-Rad (Hercules, CA) MRC1024 confocal imaging system. Cells loaded with SNARF-5F were excited at 488 nm; protonated and unprotonated SNARF-5F emission was measured at 570 and 640 nm. Imaging parameters were chosen so that neither emission channel saturated during the experiment or post-experiment calibration. Solution changes were performed manually and took place with a time constant of 4 ± 1 s (measured using fluorescent dextran in saline).

Before data acquisition, regions of interest were identified that corresponded to hair bundles, cell bodies, or background; data points for protonated and unprotonated SNARF-5F emission were acquired at 5–10 s intervals. Because of the limited amount of dye in the small volume of the bundle, the data were relatively noisy; the data were thus subjected to running three-point averaging after subtracting the background from each channel and calculating a protonated/unprotonated ratio. This running average limited the time resolution of the experiments. Ratios (R) were converted to pH using the following:

$$\mathrm{pH} = \mathrm{p}_{\mathrm{Ka}} - \log\left[\frac{\mathrm{R} - \mathrm{R}_{\mathrm{min}}}{\mathrm{R}_{\mathrm{max}} - \mathrm{R}}\right], \quad (1)$$

where R_{min} and R_{max} are the minimum and maximum ratios determined from the pH calibration. The p_{Ka} was determined from *in situ* calibration curves generated with solutions of pH 6–9 consisting of 130 mM KCl, 10 mM NaCl, 1 mM $CaCl_2$, 1 mM $MgCl_2$, 5 mM MES, and 10 μM nigericin (Invitrogen). Solutions were applied from acidic to basic, allowing at least 1 min for equilibration. The p_{Ka} for SNARF-5F in hair bundles was determined to be 7.20 ± 0.05 ($n = 14$); this value was used for all cells. R_{min} and R_{max} were measured individually for each cell using pH 6 and 9 solutions. The pH was calculated from Equation 1; for display in Figure 1, all values were normalized to the average resting pH.

We assumed that the biphasic pH kinetics after NH_4Cl removal resulted from an exponential decrease in pH attributable to NH_3 exit, characterized by a rate constant k_1 (and time constant $\tau_1 = 1/k_1$), and a coupled exponential proton extrusion with a rate k_2. The rate of change of pH is given by the following:

$$\frac{d(\mathrm{pH})}{dt} = A_1 e^{-k_1 t} - k_2(\mathrm{pH}), \quad (2)$$

where A_1 is a constant, and t is time. The solution to this equation is:

$$\Delta\mathrm{pH} = -e^{-k_2 t}\left(\frac{A_1 e^{(k_2 - k_1)t}}{k_2 - k_1} + A_2\right), \quad (3)$$

where ΔpH is the time-dependent change in pH relative to the rest pH, and A_2 is a constant. Equation 3 was used to fit data after removal of NH_4Cl; similar values for k_1 and k_2 were obtained by individually fitting the falling and rising phases of the pH response with single-exponential functions. Initial rates of H^+ extrusion were calculated by multiplying the H^+ load (25 mM) by k_2. Cells were included in the data analysis only if they acidified at least 0.5 pH units and decreased at least 0.2 pH units below the resting level after NH_4Cl removal. β_{int} corresponds to the derivative of the acid load–pH curve and was estimated by dividing the pH nadir after NH_4Cl removal in the presence of *N*-methyl-D-glucamine ($NMDG^+$) by the acid load.

Amplification of NHE isoforms from mouse inner-ear cDNA. RNA was extracted from inner ears from postnatal day 14 (P14) Black-Swiss mice using Tri-Reagent (Sigma, St. Louis, MO) following the standard protocol. First-strand cDNA was synthesized from 100 μg of total RNA primed with random hexamers using Superscript III reverse transcriptase (Invitrogen).

Conserved regions spanning introns were selected to design primers for amplification of NHE isoforms by PCR. Primers used were as follows: NHE1 (forward, TGGAGATGAAGCAGGCCATTGA; reverse, TTTGCGGATCTCTTCCTCCTTGTC; 160 bp product), NHE6 (forward, TCTCTTCGGGGAAAGTGTCCTCAAT; reverse, TAACGTCAAAGGTGTGGCTGTTGTC; 103 bp product), NHE7 (forward, GCCCCATTTTCATCATCGGAG; reverse, CCAATCTTATGCCTTCTGCCCA; 105 bp product), NHE8 (forward, GCCACTATTGCGAT-TTTCAACGC; reverse, TTGCCACCCACTGACATCTGACATA; 158 bp product), and NHE9 (forward, TGAGTTCCCGATGCTGGAGAC; reverse, GGAATCTTCTGCTTTCTGCCCAG; 365 bp product). Cycling conditions were 95°C for 90 s; 40 cycles of 94°C for 45 s, 60°C for 45 s, 72°C for 30 s; and final 5 min extension at 72°C. All products were amplified using *Taq*DNA polymerase (Promega, Madison, WI), cloned (TA cloning; Invitrogen), and sequenced.

A full-length NHE9 cDNA was cloned using Phusion DNA polymerase (MJ Research, Watertown, MA) from mouse inner-ear cDNA using GAATTCATGGCTGGGCAGCTTCGGTTTAC (forward) and CA-

GAAGCTTATTAGTCCATCTGGGGTTGACC (reverse) as primers. *Eco*RI and *Hin*dIII sites were added to facilitate cloning. Cycling conditions were as follows: 1 min at 98°C; 35 cycles of 98°C for 15 s, 68°C for 30 s, 72°C for 60 s; and a final 5 min at 72°C. PCR products were sequenced and confirmed by alignment to GenBank accession number NM_177909 (mouse NHE9/Slc9a9 full-length cDNA). Mouse NHE9 with added *Eco*RI and *Hin*dIII restriction sites was cloned into plasmid pJPA downstream from the cytomegalovirus promoter, adding C8 [PRGPDRPEGIEE (Abacioglu et al., 1994)] and enhanced green fluorescent protein (GFP) epitope tags. We also amplified mouse inner-ear NHE6 and cloned it into pJPA5 without epitope tags.

Antibody generation and characterization. NHE9 antisera were generated (Genemed Synthesis, South San Francisco, CA) using a synthetic peptide derived from mouse NHE9 with an added C-terminal cysteine (SPSPSSPTTKLALDQKSSGC). Antibodies were affinity purified as described previously (Dumont et al., 2001). Antibodies against NHE6 and their affinity purification have been described previously (Miyazaki et al., 2001); anti-NHE7 was purchased from Alpha Diagnostics (San Antonio, TX), whereas anti-NHE8 was obtained from P. Aronson (Yale University, New Haven, CT). The antibody against NHE1 was purchased from BD Biosciences Transduction Laboratories (Lexington, KY); anti-hemagglutinin (HA) was from Roche (Indianapolis, IN), and mouse monoclonal anti-C8 was a gift from Dr. T. Strassmaier (Oregon Health & Science University, Portland, OR). To further characterize the NHE6 antibody, we cloned a full-length human NHE6 (from J. Orlowski, McGill University, Montreal, Quebec, Canada), with an HA tag, into the pJPA5 expression vector.

For immunofluorescence, COS-7 cells were transfected with 0.5 μg of plasmid using 0.75 μl of Fugene 6 (Roche). After 48 h, the cells were washed with PBS and fixed in 3% formaldehyde in PBS for 20 min. After another wash in PBS, the cells were permeabilized for 15 min with 0.2% saponin in blocking solution (3% normal donkey serum and 10 mg/ml BSA in PBS) and blocked for 40 min in blocking solution without detergent. The cells were incubated for 2 h with primary antibody diluted in blocking solution (5 μg/ml anti-NHE9, anti-NHE6, anti-HA, or anti-C8), washed in PBS, and then incubated with a secondary antibody, 7.5 μg/ml cyanine 3-conjugated donkey anti-rabbit IgG or 7.5 μg/ml Alexa 488-conjugated donkey anti-mouse IgG (Invitrogen) in blocking solution for 2 h. Cells were washed, mounted, and viewed as described for immunofluorescence.

For immunoprecipitation with NHE antibodies, COS-7 cells were transfected as above. After 48 h, the cells were washed with cold PBS and incubated at 4°C for 10 min with 1% *N*-dodecyl-β-D-maltoside (Dojindo Molecular Technologies, Gaithersburg, MD) in PBS with protease inhibitors (0.2 mM PMSF, 4 μg/ml aprotinin, and 1 μg/ml leupeptin). Cells were harvested, agitated, and centrifuged to pellet nuclei. Supernatants were quantified by a BCA assay. Equal amounts of protein were diluted with the lysis solution and incubated overnight at 4°C with 2 μg of anti-NHE6, anti-NHE9, or anti-C8. Immune complexes were precipitated at room temperature with 15 μl of Protein-G Plus agarose (Santa Cruz Biotechnology, Santa Cruz, CA). After washing the beads, precipitated proteins were recovered by incubating in SDS-PAGE sample buffer containing 2% SDS and 100 mM DTT.

Inner-ear immunofluorescence. Frog saccules were isolated as described above; auditory and vestibular organs from P21 rats were dissected in MEM supplemented with 25 mM HEPES, pH 7.5. Tissue and dissociated cells were fixed, permeabilized, and blocked as described for COS cells. Tissues and cells were incubated overnight at room temperature with primary antibody (10 μg/ml anti-NHE6 or anti-NHE9, 1:500 5F10 ascites, and 5 μg/ml NHE1) in the blocking solution, washed in PBS, and incubated with 7.5 μg/ml secondary antibody and 0.25 μM fluorescent phalloidin (Invitrogen) in blocking solution for 2 h. In some experiments, the primary antibody was preincubated for 1 h at room temperature with 5 μg of antigenic peptide per microgram of antibody. Cells and tissues were washed in PBS, mounted with Vectashield (Vector Laboratories, Burlingame, CA), and viewed with a Plan Apo 60× (numerical aperture, 1.40) oil lens on a Nikon TE 300 inverted microscope with a Bio-Rad 1024 confocal imaging system. Acquired images were processed with NIH ImageJ (version 1.32j) and Photoshop (version 7.0; Adobe Systems, San Jose, CA).

Yeast plasmids, strains, and growth conditions. Mouse NHE9 was amplified using the forward primer GGCCGAGCTCATGGCTGGGCAGCTT and reverse primer GCGGAATTCTTAGTCCATCTGGGGTT, digested with *Sac*I and *Eco*RI, and cloned into the corresponding sites in the yeast expression vector pRN69 (Nass and Rao, 1998). Human liver NHE6.1 isoform was a generous gift from Dr. S. Wakabayashi (National Cardiovascular Center Research Institute, Suita, Osaki, Japan) (Miyazaki et al., 2001); this isoform carries a 96 bp insertion between Leu143 and Val144 of the original reported sequence of NHE6 (Numata et al., 1998). The open reading frame of NHE6.1 was amplified using the forward primer 5′-GCGCCGGATCCCGCTGACAGTACATACCATATAAAAATGGCTCGGCGCGGCTGGCGG-3′ and the reverse primer 5′-CGCGGGAATTCTTAGGCTGGACCATGTCTCGTATT-3′ in a PCR. The amplified product was digested with *Bam*HI and *Eco*RI and inserted into plasmid pRN69. The resulting 2μ plasmids directed the moderate overexpression of NHE6 and NHE9 under the control of tandem yeast heat shock elements (Nakamoto et al., 1991). pRin71 is also a 2μ plasmid that carries the *Saccharomyces cerevisiae NHX1* gene tagged with a C-terminal triple hemagglutinin epitope (Nass and Rao, 1998). The point mutation Y361F in *NHX1* fails to complement salt and pH growth sensitivity of the *nhx1*Δ*nha1*Δ null strain and has been described previously (Mukherjee et al., 2006).

S. cerevisiae strain AX was a derivative of BY4742 (Invitrogen); it carries a double deletion of *NHA1* and *NHX1* genes, which encode the plasma membrane and endosomal cation/proton antiporters, respectively (Brett et al., 2005b). Growth assays were performed at 30°C in APG, a synthetic minimal medium containing 10 mM arginine, 8 mM phosphoric acid, 2% glucose, 2 mM $MgSO_4$, 1 mM KCl, 0.2 mM $CaCl_2$, and trace minerals and vitamins. The pH was adjusted by addition of phosphoric acid. Seed cultures were grown in synthetic complete medium to saturation, washed three times in water, and used to seed 200 μl of APG medium in 96-well plates to a starting density of 0.05 A_{600} units/ml. Growth was monitored by measuring A_{600} after culturing for 17–24 h at 30 or 37°C, when specified.

Other methods. SDS-PAGE and immunoblotting were performed as described previously (Dumont et al., 2001). Averages and errors are reported as mean ± SE.

Results

Ca^{2+} loading increases hair-bundle H^+ concentration

To determine how PMCA activity affects hair-bundle proton pumping, we measured pH in bundles. Using a ratiometric pH-sensitive dye, SNAFL-calcein (Zhou et al., 1995), and an *in situ* p_{Ka} measurement in hair bundles, we found the resting bundle pH to be 7.35 ± 0.03 (n = 39). Depolarization opens voltage-gated Ca^{2+} channels, permitting Ca^{2+} entry into the soma (Boyer et al., 1998); some Ca^{2+} diffuses to the bundle, where PMCA extrudes it (Boyer et al., 2001) in exchange for H^+, reducing pH. Indeed, depolarizing hair cells with 20 mM KCl reduced bundle pH to 7.10 ± 0.05 (n = 18). The KCl-induced pH decrease was completely prevented (7.40 ± 0.08; n = 22) with 100 μM La^{3+}, an inhibitor of L-type Ca^{2+} channels (Kasai and Neher, 1992) and PMCA (Carafoli, 1992). These results show that Ca^{2+} loading of hair cells leads to H^+ generation in hair bundles, presumably attributable to bundle PMCA activity.

Hair bundles and somas independently transport H^+

We used a time course protocol to measure pH in regions of single hair cells during pharmacological manipulations. Because SNAFL-calcein photobleached rapidly during prolonged experiments, we switched to a more photostable pH-sensitive dye, SNARF-5F. Although the fluorescence emission from the hair bundle was relatively low (Fig. 1*G*,*H*), we could acquire images every 5–10 s for as long as 10 min without substantial photobleaching (data not shown).

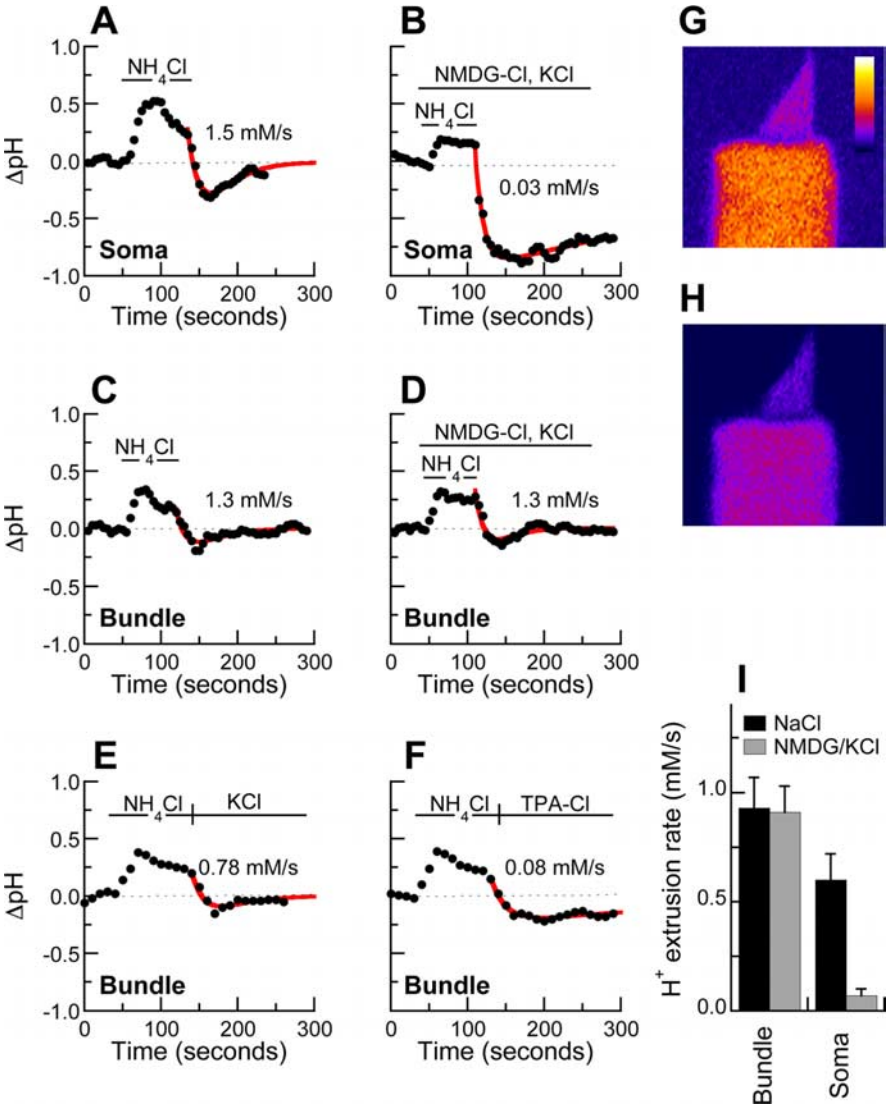

Figure 1. Dynamic pH measurements in bundles and somas of isolated hair cells. Change in pH from resting pH is plotted. ***A***, ***B***, Soma pH in response to NH_4Cl/NaCl pulse and washes with standard saline (***A***) or NMDG-Cl, 2 mM KCl, and divalent cations (***B***). ***C–F***, Hair bundle pH in response to NH_4Cl/NaCl pulse and washes with standard saline (***C***), NMDG-Cl/KCl/M^{2+} (***D***), KCl only (***E***), or TPA-Cl only (***F***). ***G***, ***H***, Protonated (***G***) and unprotonated (***H***) SNARF-5 signal in resting hair cell. Because of the low volume in the confocal section, the bundle signal is low compared with that in the soma. The linear color scale indicated in ***G*** also applies to ***H***. ***I***, Recovery rates of bundle and soma pH after acidification.

To determine how hair bundles remove H^+, we monitored the rate of pH recovery after acid load. When monitoring pH of hair-cell somas or bundles, washout of NH_4Cl with standard Na^+-containing saline led to a pH drop, often below the resting level, with a time constant of ~20 s; if acidified below resting pH, the pH of the soma and bundle recovered rapidly (Fig. 1*A*,*C*). In contrast, bundles recovered from acidification differently from somas when the wash saline contained $NMDG^+$ instead of Na^+ (Fig. 1*B*,*D*). In this solution, small amounts of other cations (K^+, Ca^{2+}, and Mg^{2+}) (Table 1) were also present. As expected for an Na^+-dependent mechanism, the soma pH recovered very slowly (Fig. 1*B*); in contrast, bundle pH quickly returned to the resting value (Fig. 1*D*). Although application of $NMDG^+$ can decrease soma pH in goldfish hair cells (Mroz and Lechene, 1993), we observed no change in resting bundle pH in response to $NMDG^+$ (data not shown). When extracellular Na^+ was present, there was no significant difference between soma (0.60 ± 0.12 mM/s; $n = 4$) and bundle (0.93 ± 0.14 mM/s; $n = 8$) recovery rates (Fig. 1*I*). In contrast, in the absence of extracellular Na^+, recovery of the soma pH (0.07 ± 0.03 mM/s; $n = 8$) was much slower than recovery in the bundle (0.91 ± 0.12 mM/s; $n = 7$). The soma recovery rate in $NMDG^+$ was significantly different ($p < 0.001$) than either the bundle recovery rate in $NMDG^+$ or the soma recovery rate in Na^+. Bundle pH recovery was similar if $NMDG^+$ was applied during and after NH_4Cl application or only after it (data not shown). Note that bundles restore their pH to the resting value under conditions in which somas remain acidic, demonstrating both that diffusion of H^+ cannot account for bundle pH homeostasis and that bundles have a mechanism for transporting H^+ across their plasma membranes.

To determine how the hair bundle maintains an appropriate H^+ concentration, we used SNARF-5F to measure pH changes during application of a weak acid, 25 mM NH_4Cl. Well characterized in other cells (Roos and Boron, 1981), NH_4Cl application first alkalinizes hair cells as NH_3 enters and binds intracellular H^+; subsequent slower entry of NH_4^+ eventually restores pH toward the resting level. Removal of NH_4Cl produces a large acidification, corresponding to an acid load of 25 mM H^+. Bundle (and soma) H^+ extrusion mechanisms then act to restore pH to the resting level.

The intrinsic buffering capacity (β_{int}) reflects the ability of a cell to buffer the influx of H^+ created by NH_4Cl application and is estimated by dividing the H^+ load by the decline in pH induced by NH_4^+ removal in the presence of $NMDG^+$ (Chesler, 2003). β_{int} values for hair-cell somas (48 ± 7 mM/pH; $n = 8$) and hair bundles (42 ± 8 mM/pH; $n = 7$) were not significantly different and were relatively high, although similar to values measured in some neurons (Ritucci et al., 1998).

We found that hair bundles could restore their pH rapidly to the resting level even if all of the extracellular cations were replaced with K^+ (Fig. 1*E*). In contrast, replacement of cation chloride salts with the bulky extracellular ion tetrapropylammonium chloride (TPA-Cl) prevented pH recovery (Fig. 1*F*).

We complemented these time course experiments with static pH measurements of hair-bundle pH, in which we determined 570/640 nm ratios from bundle regions in multiple SNARF-loaded cells, 2–3 min after NH_4Cl was removed to acidify hair cells. As a control, we saw no significant change in bundle pH after a standard saline wash in control cells (Fig. 2*A*). Moreover, we replicated the rapid recovery of bundle pH during exposure to $NMDG^+$ (Fig. 2*B*). Because the $NMDG^+$ solution also included K^+ and divalent cations (Mg^{2+} and Ca^{2+}), we removed these ions in two other experiments with $NMDG^+$. When only diva-

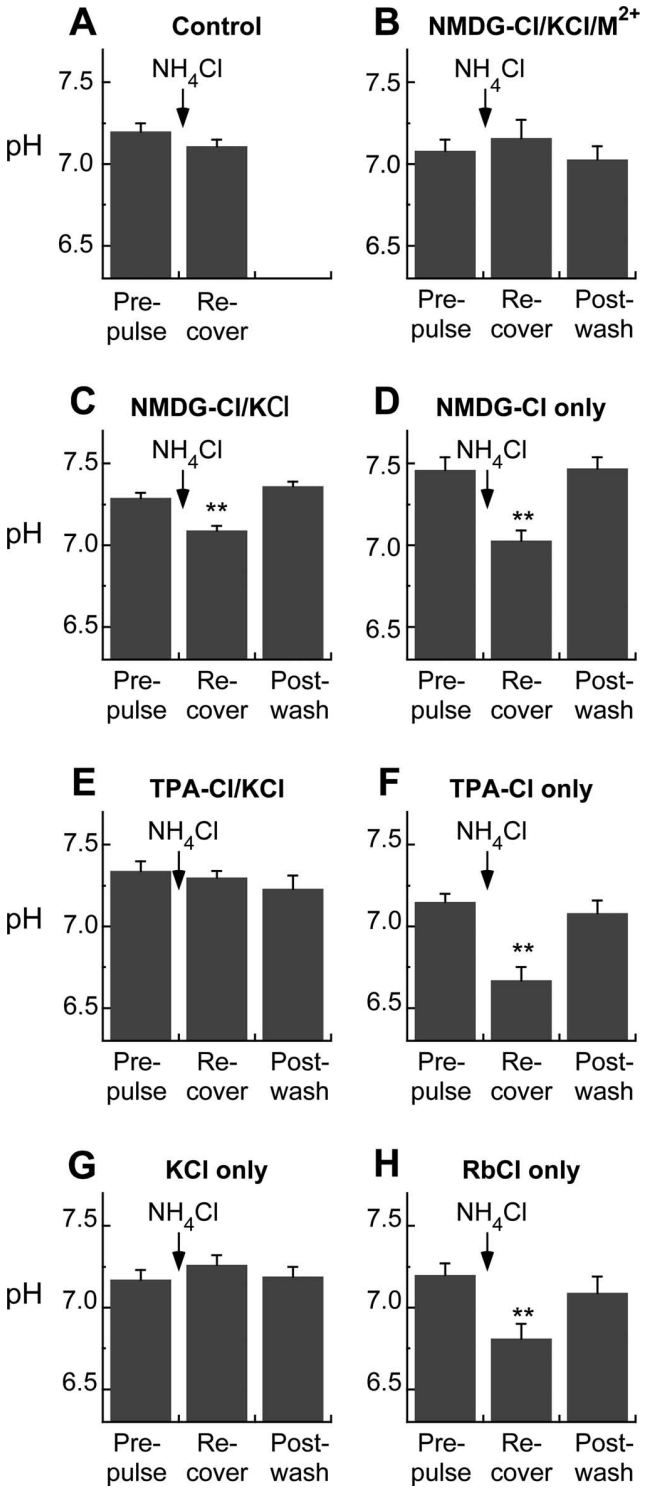

Figure 2. Static pH measurements in hair bundles of isolated hair cells. For each condition, pH was measured before (Prepulse) and 2–3 min after (Recover) a 25 mM NH_4Cl pulse; pH was subsequently measured after a wash with standard saline (Post-wash). $^{**}p < 0.001$, significance between Prepulse and Recover. Results displayed are mean ± SE from at least two dishes of isolated cells. ***A***, Standard saline recovery (no Post-wash). ***B***, NMDG-Cl/KCl/M^{2+}. ***C***, NMDG-Cl/KCl. ***D***, NMDG-Cl only. ***E***, TPA-Cl/KCl. ***F***, TPA-Cl only. ***G***, KCl only. ***H***, RbCl only.

lent cations were removed, bundles recovered somewhat less thoroughly from acidification (Fig. 2*C*). When both divalent cations and K^+ were removed, recovery from acidification was attenuated even more (Fig. 2*D*). Washing with Na^+-containing standard saline allowed complete recovery (Fig. 2*C*,*D*). Similarly, bundles recovered from a pH load in the presence of 110 mM TPA^+ and 2 mM K^+ (Fig. 2*E*); when K^+ was removed, pH recovery was inhibited (Fig. 2*F*).

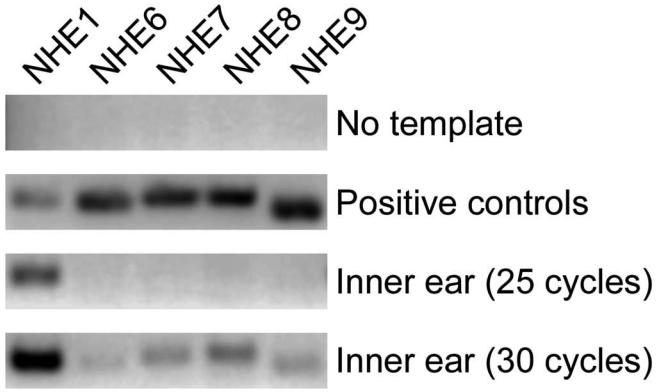

Figure 3. RT-PCR detection of NHE isoforms in mouse inner ear. NHE isoforms are indicated on top; template source is indicated on right. Positive controls were plasmids with appropriate NHE fragment. Masses of products were as expected (NHE1, 149 bp; NHE6, 145 bp; NHE7, 153 bp; NHE8, 158 bp; NHE9, 140 bp).

These results suggested that, in the absence of Na^+, K^+ was important for recovery of pH after an acid load with NH_4Cl. Indeed, hair-bundle pH recovered fully when KCl was substituted for NaCl (Fig. 2*G*). In contrast, RbCl could not substitute for KCl or NaCl (Fig. 2*H*).

Although HCO_3^- transport could play a role in hair-bundle pH homeostasis as it does in the soma (Ikeda et al., 1992), rapid pH recovery in bundles did not depend on HCO_3^-. Not only did our extracellular solutions not include HCO_3^-, but the HCO_3^-/Cl^- antiporter inhibitor 4,4-diisothiocyanatostilbene-2,2′-disulfonic acid (Romero et al., 2004) had no effect on bundle pH recovery (data not shown). Likewise, bafilomycin A_1, an inhibitor of V-type H^+-ATPases (Bowman et al., 1988), had no effect on bundle pH recovery (data not shown).

Na^+/H^+ exchangers are expressed in the mouse inner ear

Together, our data suggest that K^+/H^+ exchange is used by bundles to maintain pH. Although NHE1–NHE5 are Na^+ selective, the phylogentically related NHE6–NHE9 isoforms are thought to use either K^+ or Na^+ to transport H^+ (Orlowski and Grinstein, 2004) and, in some cases, appear transiently on the plasma membrane (Brett et al., 2002). To determine whether these isoforms were present in the inner ear, we used reverse transcription (RT)-PCR to detect NHE isoforms from inner-ear cDNA. NHE1 and NHE6–NHE9 were detected in mouse brain and kidney (data not shown); moreover, all of these NHEs were detected in mouse inner ear (Fig. 3).

Expression of NHE9 in the inner ear indicated that it was a candidate for the hair-bundle H^+ transporter. To characterize the biochemical properties of NHE9, we cloned the full-length sequence from mouse inner-ear cDNA (supplemental Fig. 1, available at www.jneurosci.org as supplemental material); this sequence matched 100% to UniProtKB/Swiss-Prot entry Q8BZ00, SL9A9_MOUSE (mouse NHE9). NHE9 showed highest similarity to NHE6 (62% identity) and NHE7 (60% identity), diverging most at the N terminus (residues 1–23 in NHE9), the second loop (residues 71–128), and two regions in the C terminus (residues 495–517 and 570–644).

We characterized NHE6 and NHE9 antibodies by detecting recombinant proteins expressed in tissue-culture cells. In immu-

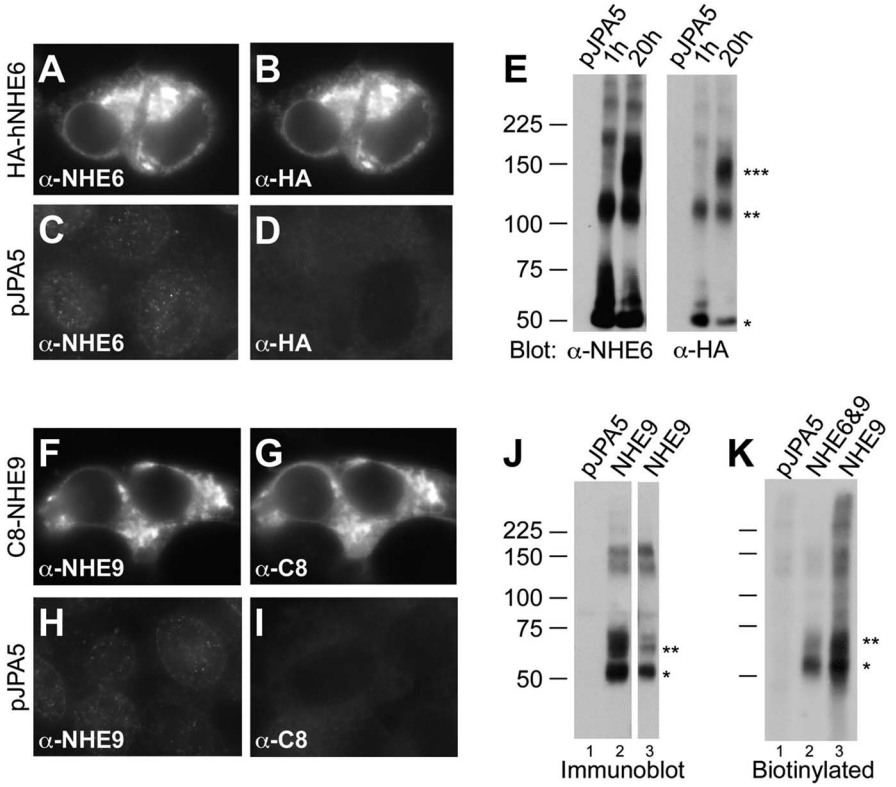

Figure 4. Specificity of NHE6 and NHE9 antibodies. ***A–D***, Immunocytochemistry with anti-NHE6. Cell expressing HA-tagged human NHE6 (***A***, ***B***) or control plasmid (***C***, ***D***) were detected with anti-NHE6 (***A***, ***C***) or anti-HA tag (***B***, ***D***) antibody. ***E***, Immunoblot with anti-NHE6. COS-7 cells expressing control plasmid (left lanes in each blot) or HA-tagged human NHE6 (right two lanes) were probed with anti-NHE6 (left blot) or anti-HA (right blot). Increased incubation of the cell extract with SDS sample buffer led to an increase in a high-molecular-weight band (***) at 20 h compared with 1 h. At shorter times, bands likely corresponding to monomer (*) and dimer (**) are most prominent. ***F–I***, Immunocytochemistry with anti-NHE9. Cell expressing C8-tagged mouse NHE9 (***F***, ***G***) or control plasmid (***H***, ***I***) were detected with anti-NHE9 (***F***, ***H***) or anti-C8 tag (***G***, ***I***). ***J***, Immunoprecipitation with anti-NHE9 (lanes 1, 2) or with anti-C8 (lane 3), followed by immunoblotting with anti-C8 (lanes 1, 2) or anti-NHE9 (lane 3). ***K***, Detection of plasma-membrane NHE9 by surface biotinylation. COS-7 cells transfected with indicated plasmids were biotinylated with a membrane-impermeable biotinylation reagent; after immunoprecipitation with anti-NHE9, proteins were detected with avidin–alkaline phosphatase.

nocytochemistry experiments, both antibodies specifically detected the appropriate recombinant transporters expressed in COS cells (Fig. 4*A–D*,*F–I*). Like other membrane proteins (Sagne et al., 1996), NHE isoforms often behave anomalously during SDS-PAGE (Miyazaki et al., 2001; Bullis et al., 2002); NHE6 and NHE9 showed similar behavior. Using anti-NHE6, we detected immunoreactive bands of 60 (*), 120 (**), and 150 kDa (***) from microsomes expressing human NHE6 (Fig. 4*E*, left), which has a calculated molecular mass of 72 kDa. Immunoblotting with an antibody that detects the HA tag on the recombinant protein demonstrated that these bands were authentic NHE6 (Fig. 4*E*, right). Incubating microsomes overnight in SDS-PAGE sample buffer enhanced the amount of 150 kDa detected (Fig. 4*E*). Because anti-NHE6 is directed against a C-terminal peptide and the HA tag is at the N terminus, bands detected corresponded to full-length NHE6. NHE9 also migrated faster in SDS-PAGE than predicted; using N-terminal (anti-C8) and C-terminal (anti-NHE9) antibodies (Fig. 4*J*), the 70 kDa mouse NHE9 tagged with C8 and GFP was detected as a prominent band at 50 kDa (*) and a doublet near 60 kDa (**). The anti-NHE9 antibody detected a single band in frog brain of a size consistent with NHE9 (supplemental Fig. 2, available at www.jneurosci.org as supplemental material). These control experiments established the specificity of our antibodies.

NHE6 and NHE9 traffic to plasma membranes

Because a hair-bundle H^+ transporter must be expressed on the plasma membrane, we examined whether, like NHE6 (Brett et al., 2002), NHE9 appeared on the surfaces of COS-7 cells. After labeling of live cells with membrane-impermeable sulfo-NHS-LC-biotin, COS cells were lysed with detergent and then subjected to immunoprecipitation with antibodies specific for expressed NHE molecules. Detection of biotinylated 60 and 120 kDa bands from mouse NHE6-expressing cells demonstrated that, like human NHE6, mouse NHE6 traffics to the plasma membrane (data not shown). Similarly, detection of biotinylated 50 and 60 kDa bands demonstrates that mouse NHE9 also appears on the plasma membrane of COS cells (Fig. 4*K*).

NHE6 and NHE9 are expressed in hair bundles

We used immunocytochemistry to determine whether NHE isoforms potentially capable of performing K^+/H^+ exchange were present in the bullfrog's inner ear. Given the role of the K^+-transporting NHEs in maintaining organelle pH, we expected to find at least one isoform present on both intracellular membranes and the hair-bundle plasma membrane. We observed no specific labeling in bullfrog saccular hair cells with antibodies against NHE7 and NHE8 (data not shown).

In contrast, an antibody against NHE6 intensely labeled hair bundles of a subset of hair cells, the central flask-shaped cells (Fig. 5*A–C*,*E*). All hair cells were labeled in the apical half of the soma (Fig. 5*C–E*), suggesting that NHE6 controls pH in intracellular organelles located there (Miyazaki et al., 2001; Brett et al., 2002). Even in this apical region, however, immunoreactivity was substantially greater in flask-shaped hair cells (Fig. 5*C*). Competition with the antigenic peptide abolished soma and bundle labeling (Fig. 5*F*).

In mammalian vestibular organs, narrow hair cells with small-diameter hair bundles are considered immature type II hair cells and are characterized by immunoreactivity for the calcium-binding protein calretinin (Dechesne et al., 1991, 1994); a subset of bullfrog saccular hair cells similarly shows high calretinin levels (Edmonds et al., 2000). In whole-mount saccules, NHE6 colocalized with calretinin immunoreactivity (Fig. 5*G*,*H*), suggesting that the NHE6-positive hair cells are immature (Chabbert, 1997).

In contrast to the sparse labeling for NHE6, an antibody against NHE9 labeled all hair bundles (Fig. 6*A*) and somas (Fig. 6*B*) of bullfrog saccules; labeling was abolished by preincubating the antibody with the antigenic peptide (Fig. 6*C*). The distribution of NHE9 in isolated cells was similar to that of bundle PMCA; both were concentrated at stereocilia tips (Fig. 6*D*) and, in some cells, in a band above the basal tapers (data not shown). Neither antibody labeled the kinocilium. NHE9 labeling also appeared in a punctate pattern throughout the hair-cell cytoplasm

(Fig. 6*E*), suggesting that it was also present on intracellular organelles, as in other cells (Nakamura et al., 2005).

An antibody specific for NHE1 labeled basolateral membranes of hair cells (Fig. 6*E*), suggesting that it is the transporter mediating Na^+-dependent H^+ extrusion from the soma. These results were consistent with previous *in situ* hybridization (Bond et al., 1998) and immunocytochemistry (Goto et al., 1999) experiments, both of which suggested that NHE1 is the Na^+/H^+ exchanger of the hair-cell soma.

NHE9 was also present in hair bundles and the cytoplasm of rat vestibular hair bundles (Fig. 7); in contrast, we did not detect NHE6 in hair bundles from rat utricle (data not shown). As in frog hair cells, NHE1 strongly labeled the basolateral membranes of rat utricle hair cells (data not shown).

NHE6 and NHE9 can mediate K^+/H^+ exchange

For NHE6 and NHE9 to extrude H^+ from hair bundles in the intact inner ear, these transporters must use K^+ as the countertransport ion. Indeed, other phylogenetically related NHE isoforms, including human NHE8, yeast Nhx1, and *Arabidopsis* NHX1, have been shown to mediate K^+/H^+ exchange (Venema et al., 2002; Brett et al., 2005b; Nakamura et al., 2005). Unfortunately, we were unable to measure acidification-dependent $^{86}Rb^+$ transport into microsomes isolated from NHE9-expressing COS-7 cells (data not shown). We therefore turned to heterologous expression of these transporters in yeast in which functional complementation approaches have proven valuable for characterizing mammalian Na^+/H^+ exchangers (Venema et al., 2002; Mukherjee et al., 2006).

Expression of NHE6 and NHE9 in a salt-sensitive yeast strain lacking two endogenous cation/proton exchangers (AX; *nhx1*Δ*nha1*Δ) initially failed to complement the growth inhibition of the host strain in medium (APG, pH 4.0) supplemented with high concentrations of NaCl or KCl (see Figs. 8*A*,*C*, 9*A*,*C*). Given the well known pH dependence of NHE activity (Orlowski and Grinstein, 2004), we reasoned that the acidic pH of yeast medium might be inhibitory for the function of mammalian NHE. Consistent with this hypothesis, both NHE6 and NHE9 were found to confer robust salt-tolerant growth in medium adjusted to pH 7.0–7.5 but not at more acidic pH (supplemental Fig. 3, available at www.jneurosci.org as supplemental material). At a physiologically relevant pH of 7.4, NHE6 expression abrogated the concentration-dependent growth-inhibiting effects of high NaCl and KCl as well as, or better than, yeast Nhx1 (Fig. 8*B*,*D*). Like yeast Nhx1, NHE6 also protected against growth inhibition by weak acids such as acetate, demonstrating a role in pH homeostasis (Fig. 8*F*), albeit only at pH 7.4.

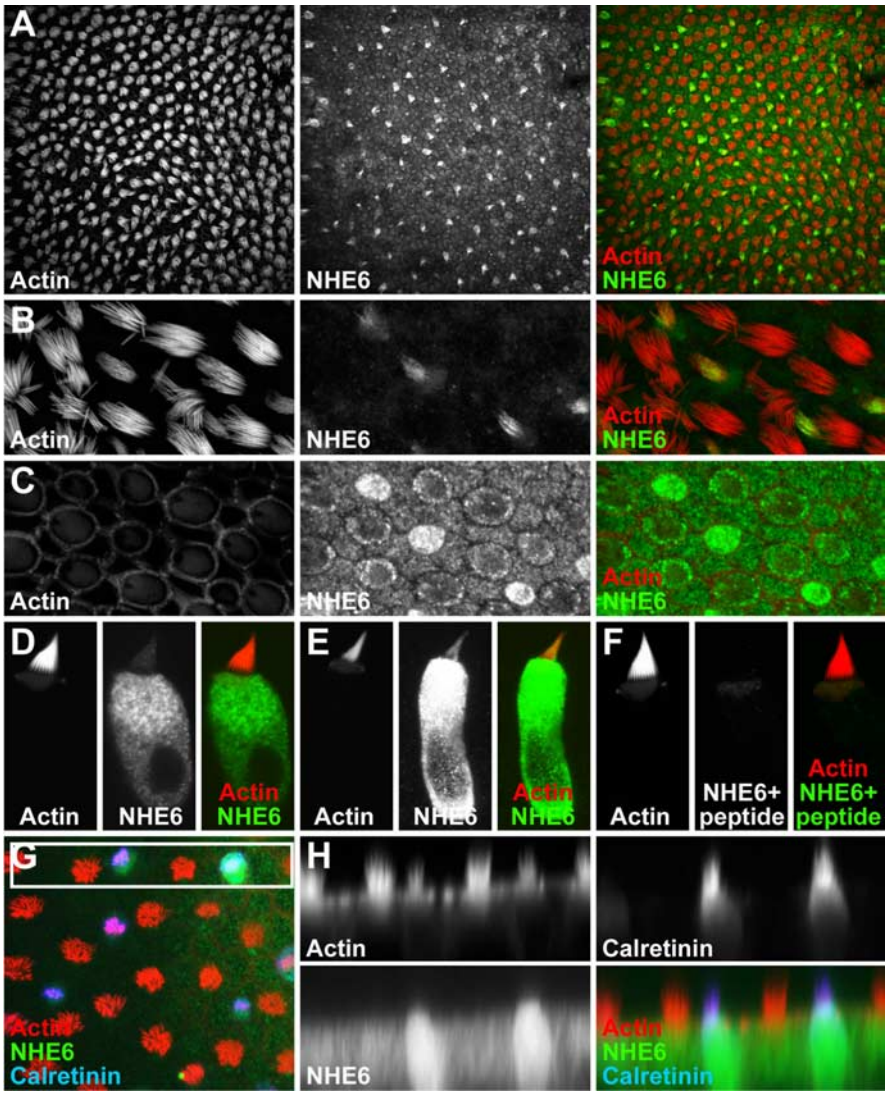

Figure 5. Localization of NHE6 in bullfrog saccule. ***A***, Low-power view of frog saccule labeled with phalloidin (for actin) and anti-NHE6. Only a small fraction of cells are positive. ***B***, High-power view of frog saccule. Small bundles are detected with anti-NHE6. ***C***, Same field as ***B*** but at the level of the cuticular plate. Cells with high levels of NHE6 in their bundles have more NHE6 in the soma. ***D***, Isolated hair cell with large hair bundle. Little NHE6 is present in the bundle. ***E***, Isolated hair cell with narrow hair bundle. NHE6 labeling is strong in the soma and modest in the bundle. ***F***, Isolated hair cell labeled after preincubation of anti-NHE6 antibody with antigenic peptide. NHE6 labeling is abolished. ***G***, Single confocal section of *z*-series triple labeled with phalloidin, anti-NHE6, and anti-calretinin. Box indicates region used for *x*–*z* reslice. ***H***, *x*–*z* reslice from *z*-series represented by ***G***. Note that cells labeled strongly with NHE6 are also positive for calretinin. Full-frame widths: ***A***, 183 μm; ***B***, ***C***, 59 μm; ***D–F***, 18 μm; ***G***, ***H***, 62 μm.

Expression of NHE9 in yeast conferred robust tolerance to NaCl and KCl at pH 7.4 but not at pH 4.0 (Fig. 9*A–D*); in contrast, complementation of Li^+ sensitivity was poor (Fig. 9*E*,*F*), similar to that of yeast Nhx1. Growth of yeast transformed with the empty vector or with plasmid expressing a point mutation in Nhx1 [shown previously to abolish ion transport (Mukherjee et al., 2006)] and was indistinguishable from that of the host strain AX. As expected, the isogenic wild-type strain, with both endogenous yeast cation/proton antiporters genes (*NHX1* and *NHA1*) intact, was more tolerant to salt stress. Unexpectedly, unlike Nhx1, NHE9 did not complement Rb^+ sensitivity of the host yeast strain, suggesting that NHE9 cannot mediate Rb^+/H^+ transport (Fig. 9*G*,*H*); this result is consistent with the failure of Rb^+ to support pH recovery in the hair bundle and suggests why the $^{86}Rb^+$ flux experiments were not successful. Together, results from yeast show that both NHE6 and NHE9 function as $K^+(Na^+)/H^+$ ex-

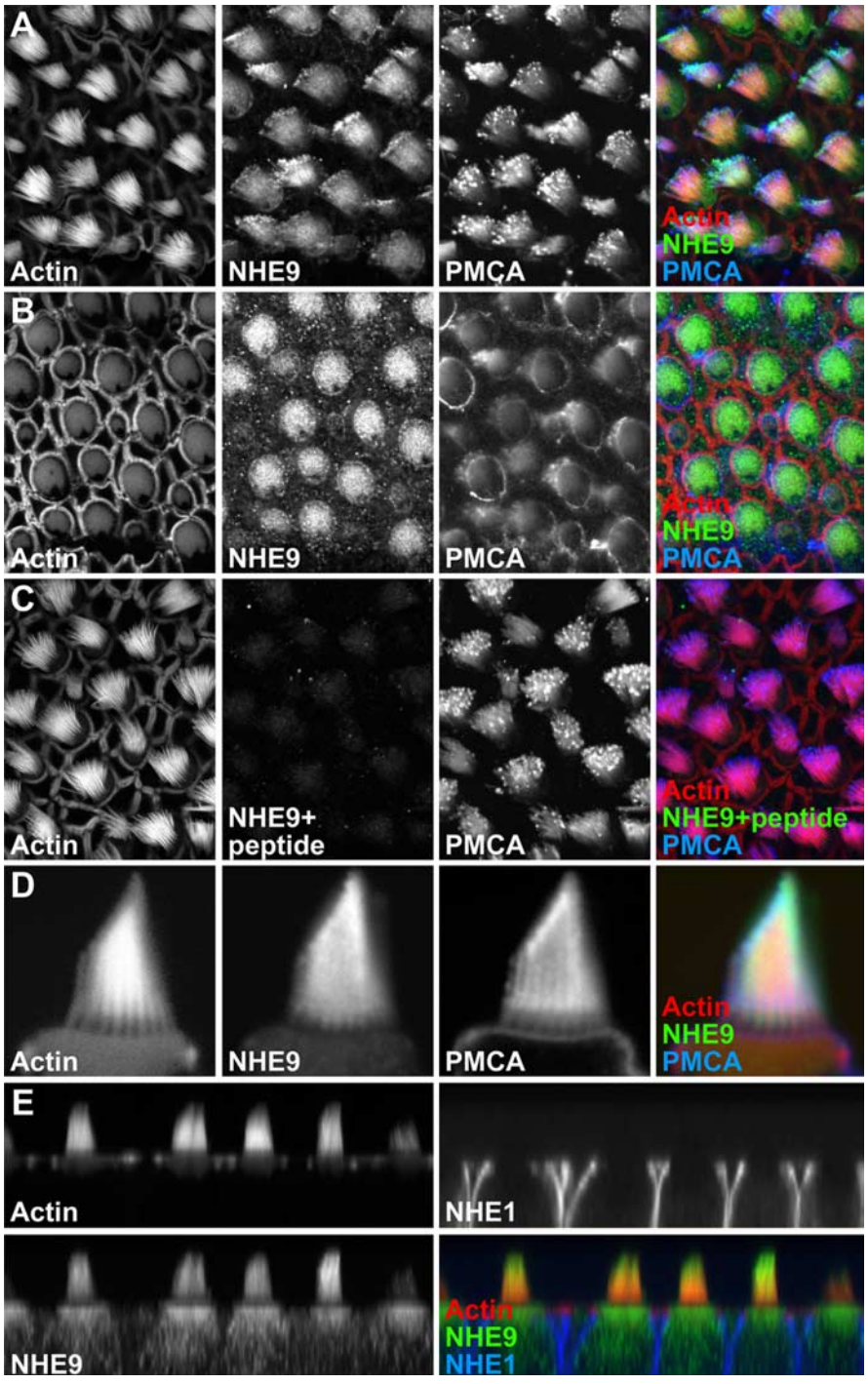

Figure 6. Localization of NHE9 in bullfrog saccule. ***A***, Low-power view of frog saccule, at level of hair bundles, labeled with phalloidin (for actin), anti-NHE9, and 5F10 (for all PMCA isoforms). All bundles have NHE9 immunoreactivity. ***B***, Same field as ***A*** but at the level of the cuticular plate. Hair cells (but not supporting cells) have substantial NHE9 immunoreactivity. ***C***, Frog saccule labeled after preincubation of anti-NHE9 antibody with antigenic peptide. NHE9 labeling is abolished. ***D***, High-power view of hair bundle from isolated frog hair cell. NHE9 labeling is throughout the bundle, with some concentration at tips of the stereocilia. ***E***, *x–z* reslice of *z*-stack of frog saccule labeled with phalloidin, anti-NHE9, and anti-NHE1. Note that NHE1 is found on hair-cell basolateral membranes. Full-frame widths: ***A–C***, 46 μm; ***D***, 10 μm; ***E***, 65 μm.

changers and that the ion preference for these transporters is K^+, $Na^+ > Li^+ \gg Rb^+$.

Discussion

The inner ear requires activity of PMCA2, the hair-bundle Ca^{2+} pump (Kozel et al., 1998; Street et al., 1998). Given a 1:1 exchange of H^+ for Ca^{2+}, the high rate of Ca^{2+} pumping inferred for bundle PMCA2 predicts a H^+ entry rate just as high (Yamoah et al., 1998). Sustained H^+ entry would eventually decrease pH sufficiently to alter activities of critical enzymes, interfering with proper mechanotransduction and other processes critical for hair-cell function.

We show here that hair bundles regulate their pH independently from the soma of the hair cell; for example, bundle pH can return to its resting level under conditions in which the soma remains acidic. Our experiments implicate a cation/proton exchanger, NHE9, as at least one of the responsible transporters; NHE9 is localized on hair bundles and apparently can use K^+ to stimulate H^+ transport. Transport by NHE9 is an appealing solution to the problem of H^+ homeostasis in hair bundles; a K^+/H^+ exchange mechanism complements the special ionic and electrical conditions present in the inner ear.

Kinetic features of H^+ extrusion by hair bundles

The resting pH of hair bundles was similar to that measured in outer hair cells (pH 7.26) (Ikeda et al., 1992) and in other cells (Roos and Boron, 1981); this value was reduced a small but significant amount after SNAFL-loaded hair cells were treated with 20 mM KCl. We suggest that the rise in H^+ occurs when voltage-gated Ca^{2+} channels open, then Ca^{2+} undergoes buffered diffusion to bundles, and finally, PMCA transports in H^+ as it pumps out Ca^{2+}.

Hair bundles also restore pH to the resting level after acid loading with 25 mM H^+ equivalents. Nevertheless, bundles likely tightly control their pH during physiological stimuli that trigger elevated hair-bundle Ca^{2+} pumping. Indeed, the rate of H^+ removal in the bundle (~1 mM/s) is at least as high as the maximum rate predicted for Ca^{2+} pumping during mechanotransduction, suggesting that the two mechanisms are well matched. Although we have not measured bundle pH during mechanotransduction, we predict that pH will remain nearly constant because of the high H^+ extrusion rate, even during large excitatory displacements that allow substantial Ca^{2+} entry.

Although many hair bundles showed substantial acidification after NH_4Cl removal, others did not. Rapid H^+ extrusion may also have contributed to this observed variability. The rate of acidification (k_1) was relatively slow and variable; if H^+ was pumped out as fast as it appears on NH_3 exit, acidification would be prevented. Indeed, in hair bundles, the value estimated for k_2 (0.04 s^{-1}) was nearly as

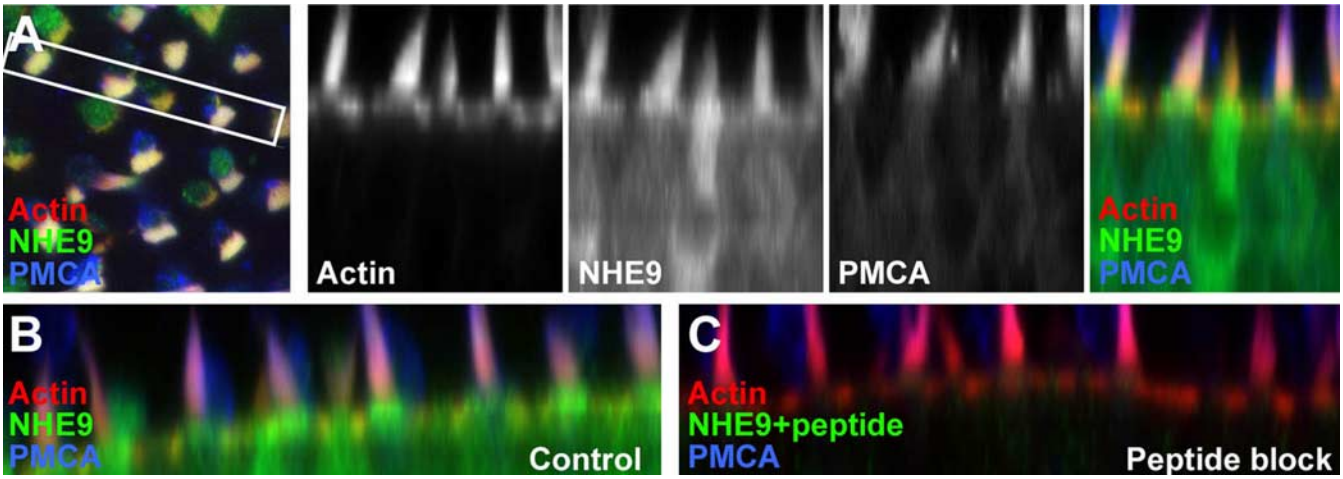

Figure 7. Localization of NHE9 in rat utricle. ***A***, Left, Single confocal section of rat utricle *z*-series triple labeled with phalloidin, anti-NHE9, and 5F10 (for PMCA). The box indicates the region used for *x–z* reslice. Right, Individual channels and merged image from *x–z* reslice. ***B***, ***C***, *x–z* reslices of rat utricles labeled with phalloidin, anti-NHE9, and 5F10 either without (***B***) or with (***C***) the NHE9 antigenic peptide. Full-panel widths: ***A***, 36 μm; ***B***, ***C***, 78 μm.

great as that for k_1 (0.06 s^{-1}). In our rate analysis, we only included cells with at least some post-NH_4Cl acidification; if this meant we systematically excluded the fastest ones, we may have substantially underestimated k_1.

H^+ buffering in hair cells and hair bundles was relatively high, suggesting that buffers can immediately control pH on H^+ entry. Strong buffering and rapid bundle H^+ efflux suggests that hair cells are optimized to handle large local H^+ fluxes in their bundles without a significant change in pH or generation of longitudinal H^+ flow.

Do bundles extrude H^+ with a K^+/H^+ exchanger?

When large extracellular cations such as $NMDG^+$ or TPA^+ are the only extracellular cations present, hair bundles cannot restore their pH to the rest level (Fig. 2*D*,*F*); in contrast, bundles remove H^+ in the presence of 124 mM K^+ and the absence of other cations (Fig. 2*G*), consistent with an active K^+/H^+ exchanger. Unexpectedly, 2 mM extracellular K^+, in the presence of high concentrations of $NMDG^+$ or TPA^+, was sufficient to restore H^+ to near its resting level (Fig. 2*B*,*C*,*E*). Antiporters with a 1:1 stoichiometry, which we assume is the case for NHE9 like NHE1 (Aronson, 1985), will reach equilibrium once the relative concentration gradients of the two substrates are balanced across the membrane. If 2 mM K^+ equilibrates H^+ across the bundle membrane and there are no other H^+ transporters, then the intracellular concentration of K^+ must be close to 2 mM, not the expected ~120 mM. In that case, leaky hair cells might have equilibrated their Na^+ and K^+ with the bathing saline; consistent with that suggestion, dissociated frog hair cells *in vitro* have high levels of intracellular Na^+ (data not shown), as also shown in cochlear hair cells (Ikeda et al., 1992; Shi et al., 2005). Alternatively, K^+ may be permissive for K^+/H^+ exchange rather than the driving force; for example, H^+ transport by NHE9 may be augmented by an electrogenic transporter that also requires K^+. Our data are thus consistent with the action of a K^+/H^+ exchanger, although they cannot establish whether NHE9 is the only H^+ transporter operating in hair bundles.

Our experiments do not address the role of H^+ transport via HCO_3^- transport (Chesler, 2003); in our experiments, hair cells successfully maintained a neutral pH in the absence of HCO_3^-, even when acidified after NH_4Cl treatment. Nevertheless, somas of outer hair cells do supplement NHE-mediated pH control with HCO_3^- mechanisms (Ikeda et al., 1992); it is possible that hair bundles do as well.

NHE6 and NHE9 as hair-bundle H^+ transporters

Given the probable participation of H^+/K^+ exchangers, NHE6 and NHE9 are compelling candidates to mediate hair-bundle H^+ transport. Both exchangers belong to a phylogenetically distinct and ancient subfamily of NHE that are ubiquitous to all eukaryotes and are thought to control pH of intracellular organelles using K^+; moreover, in other cell types, they appear on the plasma membrane on their way to their final locations on intracellular membranes (Brett et al., 2002; Goyal et al., 2005). The hair cell could harness members of this NHE subfamily for bundle pH homeostasis by allowing their trafficking to the apical membrane but preventing their rapid endocytosis, trapping the transporters on the bundle membrane. Both NHE6 and NHE9 are abundant on hair-cell intracellular organelles, however, suggesting that apical retention of these transporters is modest. This localization contrasts strikingly with that of NHE1, which appears to be targeted nearly exclusively to the basolateral membranes of hair cells.

We found NHE6 only in a subset of bullfrog saccular hair cells, suggesting that this transporter plays a specialized role. Little is known about the function of hair cells with small-diameter hair bundles, in which NHE6 is primarily localized. Strong immunoreactivity for calretinin is reminiscent of developing type II cells of the mammalian vestibular system (Dechesne et al., 1994), suggesting that NHE6 might only appear transiently in hair cells during development.

In contrast, NHE9 is present in all bundles, consistent with it being the primary bundle H^+ transporter in mature hair cells. NHE9 primarily colocalizes in hair bundles with PMCA, with both transporters concentrated at stereocilia tips. Because Ca^{2+} will enter bundles through mechanotransduction channels located at tips, localization of the PMCA there, as well as the primary H^+ transporter that responds to PMCA activity, is physiologically appropriate.

Ion selectivity of NHE6 and NHE9

NHE isoforms residing primarily or exclusively at the plasma membrane (NHE1–NHE5) are Na^+ selective and do not translocate K^+ ions. In contrast, it has been proposed that the more

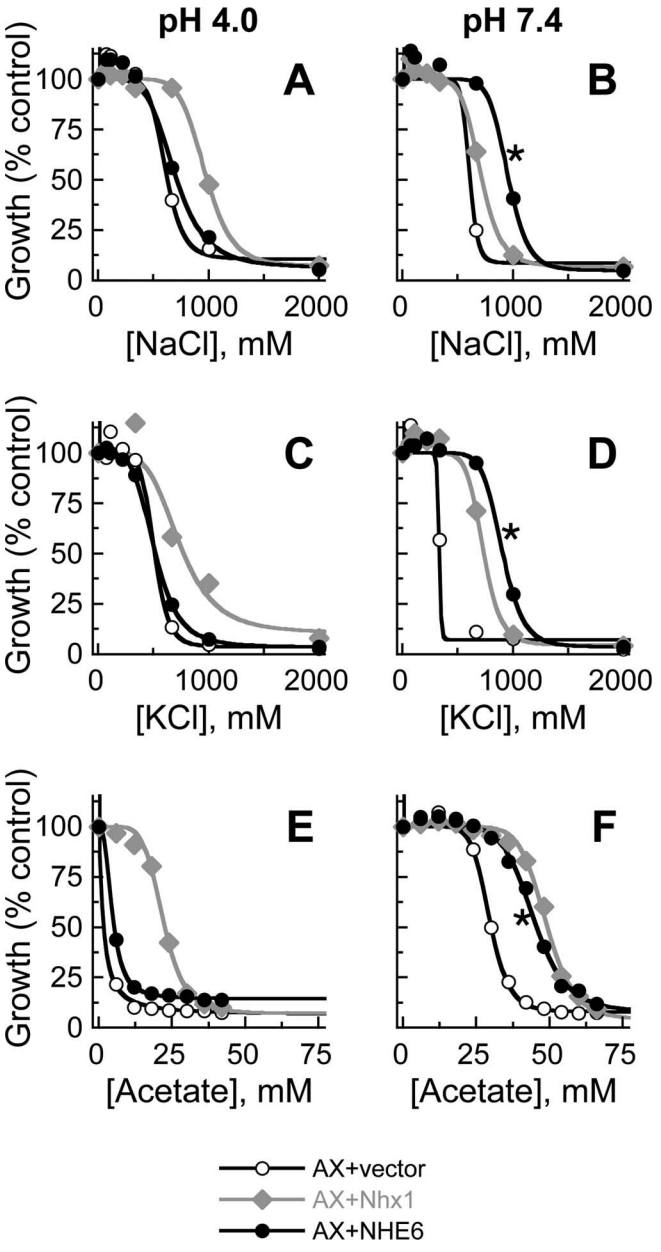

Figure 8. NHE6 expression reduces sensitivity of yeast growth to salt and weak acid stress. AX strain (lacking *NHA1* and *NHX1* ion transporters) was transformed with empty vector, yeast Nhx1, or human NHE6. Growth was assessed in the presence of varying concentrations of the following: ***A***, NaCl at pH 4.0; ***B***, NaCl at pH 7.4; ***C***, KCl at pH 4.0; ***D***, KCl at pH 7.4; ***E***, sodium acetate at pH 4.0; and ***F***, sodium acetate at pH 7.4. NHE6 rescued the slow-growth phenotype at pH 7.4 (*). Data points are averages of eight replicates combined from two independent experiments. Nearly identical results were obtained with two independently transformed clones of NHE6.

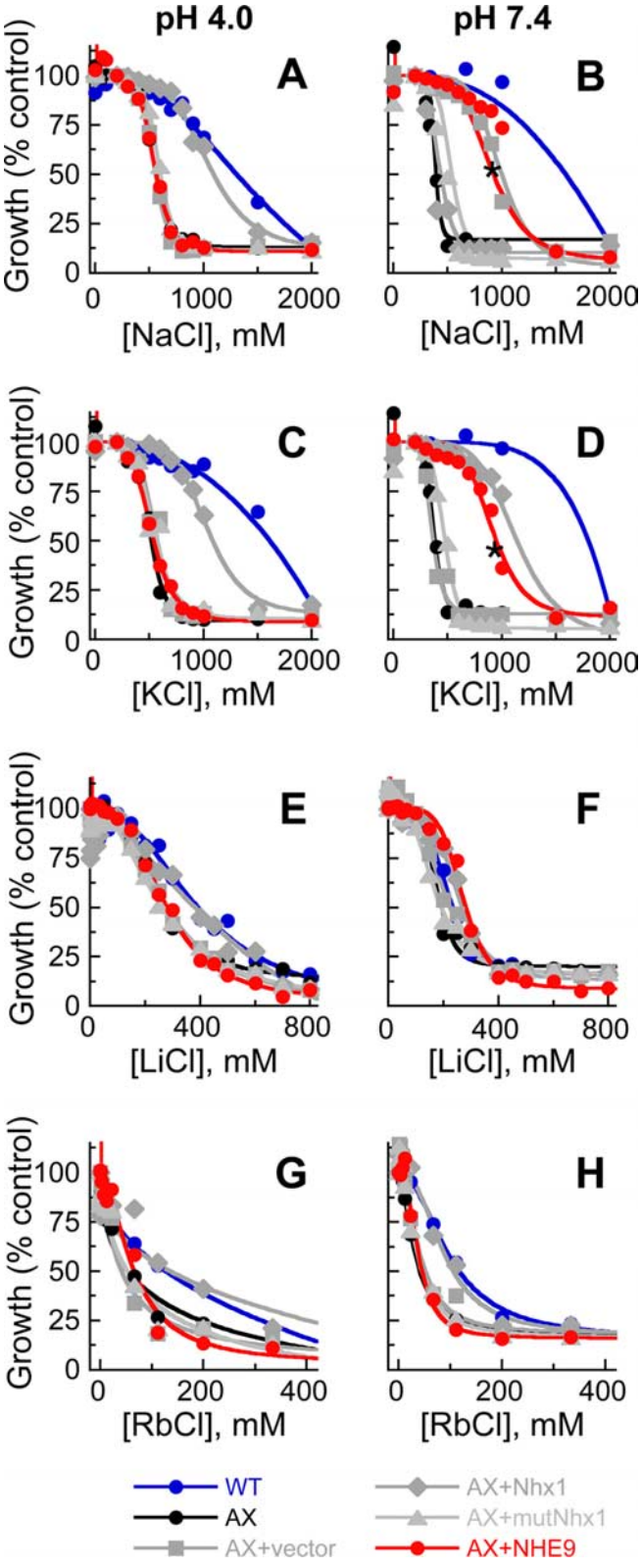

Figure 9. NHE9 expression reduces sensitivity of yeast growth to salt. AX strain was transformed with empty vector, yeast Nhx1, mutant Y361F Nhx1, or mouse NHE9. Growth of wild type yeast (WT), AX, or transformants was assessed in the presence of varying concentrations of the following: ***A***, NaCl at pH 4.0; ***B***, NaCl at pH 7.4; ***C***, KCl at pH 4.0; ***D***, KCl at pH 7.4; ***E***, LiCl at pH 4.0; ***F***, LiCl at pH 7.4; ***E***, RbCl at pH 4.0; and ***F***, RbCl at pH 7.4. NHE9 rescued the slow-growth phenotype at pH 7.4 (*). Data points are averages of two to four replicates.

recently identified organellar NHE isoforms (NHE6–NHE9) would primarily rely on K^+, abundant in the cytoplasm, for countertransport with luminal H^+ (Brett et al., 2005a). Consistent with this hypothesis, cation tolerance growth assays in yeast suggested that NHE6 and NHE9 can mediate both Na^+/H^+ and K^+/H^+ transport. Expression of NHE9 conferred only a modest protection against LiCl toxicity, as was found for yeast Nhx1, suggesting that Li^+ is a poor substrate for these NHEs. Surprisingly, unlike yeast Nhx1, expression of NHE6 and NHE9 failed to confer growth tolerance to RbCl in yeast, suggesting that the transport pathway of these NHEs may be more restrictive to ions

of larger radius. These results contrast those with NHE7, which mediates H^+-dependent $^{86}Rb^+$ influx into microsomes (Numata and Orlowski, 2001). Moreover, because hair bundles fail to remove H^+ when Rb^+ is the only extracellular cation, the yeast noncomplementation results support the proposal that NHE9 mediates bundle H^+ transport.

Value of K^+/H^+ exchange to the hair cell

K^+/H^+ exchange is a particularly elegant solution for H^+ removal from the hair bundle (supplemental Fig. 4, available at www.jneurosci.org as supplemental material). Because NHE-mediated H^+ extrusion does not require ATP, the hair cell only expends ATP to mediate Ca^{2+}/H^+ exchange by PMCA. Moreover, local recycling of H^+ in the hair bundle avoids the need for additional H^+ pumping from the soma into the endolymph, which would be required to balance any H^+ that diffused from the bundle to the soma and out into perilymph. Activity of the NHEs requires net K^+ influx. Because K^+ is the major charge carrier during mechanotransduction, additional entering K^+ would use the well established pathway for K^+ recycling (Wangemann, 2002). Moreover, NHE-mediated K^+/H^+ exchange is electroneutral, so H^+ transport would not be sensitive to changes in the membrane potential of the hair cell or the large endocochlear potential. The driving force for H^+ extrusion is not the electrochemical gradients for H^+, K^+, or Na^+ but instead their chemical gradients. Because the concentration of K^+ (and Na^+) is approximately the same on either side of the hair-bundle plasma membrane, electroneutral transport mediated by NHEs allows the bundle to respond selectively to an imbalance in the concentration of H^+ imparted by PMCA activity. The bundle can thus restore pH to the resting level without energy expenditure by the cell.

References

Abacioglu YH, Fouts TR, Laman JD, Claassen E, Pincus SH, Moore JP, Roby CA, Kamin-Lewis R, Lewis GK (1994) Epitope mapping and topology of baculovirus-expressed HIV-1 gp160 determined with a panel of murine monoclonal antibodies. AIDS Res Hum Retroviruses 10:371–381.

Aronson PS (1985) Kinetic properties of the plasma membrane Na^+-H^+ exchanger. Annu Rev Physiol 47:545–560.

Blair HC, Teitelbaum SL, Ghiselli R, Gluck S (1989) Osteoclastic bone resorption by a polarized vacuolar proton pump. Science 245:855–857.

Bond BR, Ng LL, Schulte BA (1998) Identification of mRNA transcripts and immunohistochemical localization of Na/H exchanger isoforms in gerbil inner ear. Hear Res 123:1–9.

Bowman EJ, Siebers A, Altendorf K (1988) Bafilomycins: a class of inhibitors of membrane ATPases from microorganisms, animal cells, and plant cells. Proc Natl Acad Sci USA 85:7972–7976.

Boyer C, Lehouelleur J, Sans A (1998) Potassium depolarization of mammalian vestibular sensory cells increases $[Ca^{2+}]_i$ through voltage-sensitive calcium channels. Eur J Neurosci 10:971–975.

Boyer C, Art JJ, Dechesne CJ, Lehouelleur J, Vautrin J, Sans A (2001) Contribution of the plasmalemma to Ca^{2+} homeostasis in hair cells. J Neurosci 21:2640–2650.

Brett CL, Wei Y, Donowitz M, Rao R (2002) Human Na^+/H^+ exchanger isoform 6 is found in recycling endosomes of cells, not in mitochondria. Am J Physiol Cell Physiol 282:C1031–C1041.

Brett CL, Donowitz M, Rao R (2005a) Evolutionary origins of eukaryotic sodium/proton exchangers. Am J Physiol Cell Physiol 288:C223–C239.

Brett CL, Tukaye DN, Mukherjee S, Rao R (2005b) The yeast endosomal Na^+K^+/H^+ exchanger Nhx1 regulates cellular pH to control vesicle trafficking. Mol Biol Cell 16:1396–1405.

Bullis BL, Li X, Singh DN, Berthiaume LG, Fliegel L (2002) Properties of the Na^+/H^+ exchanger protein. Detergent-resistant aggregation and membrane microdistribution. Eur J Biochem 269:4887–4895.

Carafoli E (1992) The Ca^{2+} pump of the plasma membrane. J Biol Chem 267:2115–2118.

Chabbert CH (1997) Heterogeneity of hair cells in the bullfrog sacculus. Pflügers Arch 435:82–90.

Chesler M (2003) Regulation and modulation of pH in the brain. Physiol Rev 83:1183–1221.

Dechesne CJ, Winsky L, Kim HN, Goping G, Vu TD, Wenthold RJ, Jacobowitz DM (1991) Identification and ultrastructural localization of a calretinin-like calcium-binding protein (protein 10) in the guinea pig and rat inner ear Brain Res 560:139–148.

Dechesne CJ, Rabejac D, Desmadryl G (1994) Development of calretinin immunoreactivity in the mouse inner ear. J Comp Neurol 346:517–529.

Dumont RA, Lins U, Filoteo AG, Penniston JT, Kachar B, Gillespie PG (2001) Plasma membrane Ca^{2+}-ATPase isoform 2a is the PMCA of hair bundles. J Neurosci 21:5066–5078.

Edmonds B, Reyes R, Schwaller B, Roberts WM (2000) Calretinin modifies presynaptic calcium signaling in frog saccular hair cells. Nat Neurosci 3:786–790.

Goto S, Oshima T, Ikeda K, Takasaka T (1999) Expression and localization of the Na^+-H^+ exchanger in the guinea pig cochlea. Hear Res 128:89–96.

Goyal S, Mentone S, Aronson PS (2005) Immunolocalization of NHE8 in rat kidney. Am J Physiol Renal Physiol 288:F530–F538.

Hao L, Rigaud JL, Inesi G (1994) Ca^{2+}/H^+ countertransport and electrogenicity in proteoliposomes containing erythrocyte plasma membrane Ca-ATPase and exogenous lipids. J Biol Chem 269:14268–14275.

Hill JK, Williams DE, LeMasurier M, Dumont RA, Strehler EE, Gillespie PG (2006) Splice-site A choice targets plasma-membrane Ca^{2+}-ATPase isoform 2 to hair bundles. J Neurosci 26:6172–6180.

Hirono M, Denis CS, Richardson GP, Gillespie PG (2004) Hair cells require phosphatidylinositol 4,5-bisphosphate for mechanical transduction and adaptation. Neuron 44:309–320.

Ikeda K, Saito Y, Nishiyama A, Takasaka T (1992) Intracellular pH regulation in isolated cochlear outer hair cells of the guinea-pig. J Physiol (Lond) 447:627–648.

Kasai H, Neher E (1992) Dihydropyridine-sensitive and omega-conotoxin-sensitive calcium channels in a mammalian neuroblastoma-glioma cell line. J Physiol (Lond) 448:161–188.

Kozel PJ, Friedman RA, Erway LC, Yamoah EN, Liu LH, Riddle T, Duffy JJ, Doetschman T, Miller ML, Cardell EL, Shull GE (1998) Balance and hearing deficits in mice with a null mutation in the gene encoding plasma membrane Ca^{2+}-ATPase isoform 2. J Biol Chem 273:18693–18696.

Miyazaki E, Sakaguchi M, Wakabayashi S, Shigekawa M, Mihara K (2001) NHE6 protein possesses a signal peptide destined for endoplasmic reticulum membrane and localizes in secretory organelles of the cell. J Biol Chem 276:49221–49227.

Mroz EA, Lechene C (1993) Extracellular *N*-methyl-D-glucamine leads to loss of hair-cell sodium, potassium, and chloride. Hear Res 70:146–150.

Mukherjee S, Kallay L, Brett CL, Rao R (2006) Mutational analysis of the intramembranous H10 loop of yeast Nhx1 reveals a critical role in ion homeostasis and vesicle trafficking. Biochem J 398:97–105.

Nakamoto RK, Rao R, Slayman CW (1991) Expression of the yeast plasma membrane $[H^+]$ATPase in secretory vesicles. A new strategy for directed mutagenesis. J Biol Chem 266:7940–7949.

Nakamura N, Tanaka S, Teko Y, Mitsui K, Kanazawa H (2005) Four Na^+/H^+ exchanger isoforms are distributed to Golgi and post-Golgi compartments and are involved in organelle pH regulation. J Biol Chem 280:1561–1572.

Nass R, Rao R (1998) Novel localization of a Na^+/H^+ exchanger in a late endosomal compartment of yeast. Implications for vacuole biogenesis. J Biol Chem 273:21054–21060.

Numata M, Orlowski J (2001) Molecular cloning and characterization of a novel $(Na^+,K^+)/H^+$ exchanger localized to the trans-Golgi network. J Biol Chem 276:17387–17394.

Numata M, Petrecca K, Lake N, Orlowski J (1998) Identification of a mitochondrial Na^+/H^+ exchanger. J Biol Chem 273:6951–6959.

Orlowski J, Grinstein S (2004) Diversity of the mammalian sodium/proton exchanger SLC9 gene family. Pflügers Arch 447:549–565.

Ritucci NA, Chambers-Kersh L, Dean JB, Putnam RW (1998) Intracellular pH regulation in neurons from chemosensitive and nonchemosensitive areas of the medulla. Am J Physiol 275:R1152–R1163.

Romero MF, Boron WF (1999) Electrogenic Na^+/HCO_3^- cotransporters: cloning and physiology. Annu Rev Physiol 61:699–723.

Romero MF, Fulton CM, Boron WF (2004) The SLC4 family of HCO_3^- transporters. Pflügers Arch 447:495–509.

Roos A, Boron WF (1981) Intracellular pH. Physiol Rev 61:296–434.

Sagne C, Isambert MF, Henry JP, Gasnier B (1996) SDS-resistant aggregation of membrane proteins: application to the purification of the vesicular monoamine transporter. Biochem J 316:825–831.

Salvador JM, Inesi G, Rigaud JL, Mata AM (1998) Ca^{2+} transport by reconstituted synaptosomal ATPase is associated with H^+ countertransport and net charge displacement. J Biol Chem 273:18230–18234.

Shi X, Gillespie PG, Nuttall AL (2005) Na^+ influx triggers bleb formation on inner hair cells. Am J Physiol Cell Physiol 288:C1332–C1341.

Silver RB, Soleimani M (1999) H^+-K^+-ATPases: regulation and role in pathophysiological states. Am J Physiol 276:F799–F811.

Street VA, McKee-Johnson JW, Fonseca RC, Tempel BL, Noben-Trauth K (1998) Mutations in a plasma membrane Ca^{2+}-ATPase gene cause deafness in deafwaddler mice. Nat Genet 19:390–394.

Venema K, Quintero FJ, Pardo JM, Donaire JP (2002) The *Arabidopsis* Na^+/H^+ exchanger AtNHX1 catalyzes low affinity Na^+ and K^+ transport in reconstituted liposomes. J Biol Chem 277:2413–2418.

Wangemann P (2002) K^+ cycling and the endocochlear potential. Hear Res 165:1–9.

Yamoah EN, Lumpkin EA, Dumont RA, Smith PJ, Hudspeth AJ, Gillespie PG (1998) Plasma membrane Ca^{2+}-ATPase extrudes Ca^{2+} from hair cell stereocilia. J Neurosci 18:610–624.

Zhou Y, Marcus EM, Haugland RP, Opas M (1995) Use of a new fluorescent probe, seminaphthofluorescein-calcein, for determination of intracellular pH by simultaneous dual-emission imaging laser scanning confocal microscopy. J Cell Physiol 164:9–16.